journal

Correlation Between Photoluminescence and Structural Defects in Ca$_{1+x}$Cu$_{3-x}$Ti$_4$O$_{12}$ Systems

Larissa H. Oliveira,[‡,†] Elaine C. Paris,[§] Waldir Avansi,[¶] Miguel A. Ramirez,[∥] Valmor R. Mastelaro,[††] Elson Longo,[¶] and José A. Varela[¶]

[‡]DQ/UFSCar-Universidade Federal de São Carlos, São Carlos 13565-905, SP, Brazil

[§]EMBRAPA Instrumentação Agropecuária, 13560-970 CP 741 São Carlos, SP, Brazil

[¶]UNESP-Universidade Estadual Paulista, Araraquara 14801-907, SP, Brazil

[∥]UNESP-Universidade Estadual Paulista, Guaratinguetá 12516-410, SP, Brazil

[††]IFSC-USP, Universidade de São Paulo, São Carlos 13560-970, SP, Brazil

Ca$_{1+x}$Cu$_{3-x}$Ti$_4$O$_{12}$ powders were synthesized by a conventional solid-state reaction. X-ray diffraction (XRD) was performed to verify the formation of cubic CaCu$_3$Ti$_4$O$_{12}$ (CCTO) and ortho-rhombic CaTiO$_3$ (CTO) phases at long range. Rietveld refinements indicate that excess Ca atoms added to the Ca$_{1-x}$Cu$_{3-x}$Ti$_4$O$_{12}$ ($x = 1.0$) composition segregated in a CaTiO$_3$ secondary phase suggesting that solubility limit of Ca atoms in the CaCu$_3$Ti$_4$O$_{12}$ lattice was reached for this system. The FE-SEM images show that the Ca$_{1+x}$Cu$_{3-x}$Ti$_4$O$_{12}$ ($0 < x < 3$) powders are composed of several agglomerated particles with irregular morphology. X-ray absorption near-edge structure spectroscopy (XANES) spectra indicated [TiO$_5$V$_o^z$]-[TiO$_6$] complex clusters in the CaCu$_3$Ti$_4$O$_{12}$ structure which can be associated with oxygen vacancies (V$_o^z$ = V$_o^x$, V$_o^•$, and V$_o^{••}$) whereas in the CaTiO$_3$ powder, this analysis indicated [TiO$_6$]–[TiO$_6$] complex clusters in the structure. Ultraviolet-visible (UV–vis) spectra and photoluminescence (PL) measurements for the analyzed systems revealed structural defects such as oxygen vacancies, distortions, and/or strains in CaCu$_3$Ti$_4$O$_{12}$ and CaTiO$_3$ lattices, respectively.

I. Introduction

IN recent years, ATiO$_3$-type perovskites (where A = Ca, Sr, Ba, or Pb) are considered as the key materials for applications in electronic devices due to their interesting electrical properties.[1] While studying dielectric properties of ACu$_3$Ti$_4$O$_{12}$ (A = metallic ions) perovskite-type materials in 2000, Subramanian *et al.*[2] noticed that the cubic CaCu$_3$Ti$_4$O$_{12}$ perovskite had an electrical permittivity of 10.826. This is constant in the range of 100 to 400 K (above 1 MHz).

The first group of researchers attributed the dielectric permittivity of CaCu$_3$Ti$_4$O$_{12}$ to grain boundaries and defects related to its microstructure.[2–5] However, another group of researchers argued that its origin is due to extrinsic mechanisms such as twins, grain boundary, segregation of CuO in the grain boundary, electrodes, etc.[6–9] Bueno *et al.*[10] proposed another model which explains their unusually high dielectric constant and considered that an internal barrier layer capacitance mechanism is responsible for this phenome-

non. In this model, it is proposed that these barriers operate in the nanoscale range due to polaron defects associated with a stacking fault. This mechanism is referred to as nanoscale barrier layer capacitance. Nevertheless, the formation mechanism, detailed structures, and properties of these domains have not yet been clarified.

In addition to its high dielectric permittivity, CaCu$_3$Ti$_4$O$_{12}$ exhibits a strong nonlinear current-voltage behavior. Chung *et al.*[11] observed a strong nonlinear current-voltage behavior for this material, and found a nonlinear coefficient value (α^i) of 912 in the range of 5–100 mA.[12,13] Microelectrodes were placed on the surface of a CaCu$_3$Ti$_4$O$_{12}$ sample sintered for 20 h. From electrical measurements, it was concluded that electrostatic barriers are formed in the grain boundary which causes the nonohmic behavior, which allows its application as a varistor material alloy.

Due to these remarkable properties, CaCu$_3$Ti$_4$O$_{12}$ is being considered as a promising material for applications in microelectronics, mainly for capacitive components. On the other hand, the dielectric loss of this material is slightly high which precludes its application in this area.[13] Thus, an effective means to improve these dielectric properties has been to dope the main crystalline phase with La$_2$O$_3$,[14] VO$_2$,[15] SrO$_2$,[16] MgO,[17] Eu$_2$O$_3$,[18] ZnO,[19] ZrO$_2$,[20] TiO$_2$,[21] or SnO$_2$.[22] Li *et al.*[23] studied the electrical properties of Ca$_{1+x}$Cu$_{3-x}$Ti$_4$O$_{12}$ ceramics prepared by the solid-state reaction method. These researchers observed that the secondary CaTiO$_3$ phase is found in the grain boundary, and the excess of Ca favored nonohmic properties.

In addition to dielectric and nonohmic properties, the CCTO ceramic material can be employed as a gas sensor and for photoluminescent devices.[24,25] Very little research has been reported in the literature on PL properties of this ceramic oxide.

Parra *et al.*[25] observed PL emission bands at 544 and 800 nm in CCTO-based films synthesized by a sol–gel method. The two emission bands were attributed to [TiO$_5$Vo^z], [CuO$_{11}$Vo^z], and [CaO$_{11}$Vo^z] complex clusters, where Vo^z represents oxygen vacancies V$_o^x$, V$_o^•$, and V$_o^{••}$ in the structure. However, the authors reported limited information on the origin of the optical property in this material.

The appearance of a PL response is very important in the investigation of energy levels in materials because it provides important information about the physical and chemical properties of materials at the molecular level, including

[i]The alpha coefficient is the reverse of angular coefficient in *E* versus *J* curve, and has been used to characterize some materials with potential varistor application. This coefficient can be calculated according to Clarke.[13]

shallow and deep defects at the band gap.[26] Thus, in this work, we report the successful preparation of $Ca_{1+x}Cu_{3-x}Ti_4O_{12}$ ($x = 0.0$, 1.0 and 3.0) powders by a conventional solid-state reaction. In addition, we propose a structural model to explain PL properties for this ceramic oxide.

II. Experimental Method

(1) Synthesis of $Ca_{1+x}Cu_{3-x}Ti_4O_{12}$ ($0 \leq x \leq 3$) Ceramic Powders

$CaCu_3Ti_4O_{12}$ (CCTO($x = 0$)), $Ca_2Cu_2Ti_4O_{12}$ (CCTO/CTO ($x = 1$)), and $CaTiO_3$ (CTO($x = 3$)) ceramic powders were prepared using a solid-state reaction. Thus, a stoichiometric quantity of TiO_2, CuO, and $CaCO_3$ (99.99%; Aldrich) were ball milled in isopropyl alcohol in a polyethylene bottle using zirconia balls. The powders were milled for 24 h; after alcohol evaporation, the powders were homogenized in a mortar and then sieved using a granular sieve of 200 mesh. Then these compositions were heated at 900°C for 12 h in a conventional furnace using a heating rate of 5°C/min.

(2) Characterization

CCTO($x = 0$), CCTO/CTO($x = 1$), and CTO($x = 3$) powders were structurally characterized by XRD in a Rietveld routine using a Rigaku-DMax/2500PC diffractometer (Tokyo, Japan) with $CuK\alpha$ radiation ($\lambda = 1.5406$ Å) and in the 2θ range from 10° to 110° with a scanning rate of 0.02°/min. FE-SEM analyses were performed in back-scattering electron mode (BSE) using a scanning electron microscope (JSM-6460LV microscope; Jeol, Tokyo, Japan). The compositional analysis as well as the mapping of the elements in the analyzed samples was performed by means of energy dispersive X-ray spectroscopy (EDXS) analysis. XANES spectra were measured at the titanium (Ti) K-edge using the D08B-XAFS2 beam line at the Brazilian Synchrotron Light Laboratory (LNLS). Ti K-edge XANES spectra were collected in the range of 4910–5100 eV using an energy step of 0.5 eV and an integration time of 3 s. Analyses of XANES spectra were performed using the IFEFFIT package.[27,28] UV–vis absorption spectra of $Ca_{1+x}Cu_{3-x}Ti_4O_{12}$ powders were performed using VARIAN Cary 5G Spectrophotometer. The PL was measured with a 139 Thermal Jarrel-Ash Monospec 27 monochromator (Horiba, Kyoto, Japan) and a Hamamatsu R446 photomultiplier (Hamamatsu, Shimokanzo, Iwata City, Japan). The 350.7 nm exciting wavelength of a krypton ion laser (Coherent Innova, Santa Clara, CA) was used; a nominal output power of 200 mW was maintained. All measurements were performed at room temperature.

III. Results and Discussion

(1) XRD Measurements and Rietveld Refinement

Figures 1(a)–(c) show XRD patterns of the $Ca_{1+x}Cu_{3-x}Ti_4O_{12}$ ($0 > x > 3$) ceramic powders, where diffraction peaks of the CCTO system [see Fig.1(a)] are of a $CaCu_3Ti_4O_{12}$ cubic perovskite with a space group $Im\text{-}3$ which is in agreement with the respective Inorganic Crystal Structure Database (ICSD) card no. 95-714. Increasing the amount of Ca ($x = 1.0$) produces a secondary phase identified as a perovskite-type $CaTiO_3$ orthorhombic structure and a space group $Pbnm$ in accordance with its respective ICSD card no. 74-212. In the CTO system, diffraction peaks related to the $CaCu_3Ti_4O_{12}$ are absent as expected, and only the diffraction peaks related to the $CaTiO_3$ phase were detected. All XRD results are in agreement with the literature.[29–31]

The Rietveld refinement method was performed with the specific objective to analyze the influence of excess calcium atoms in $Ca_{1+x}Cu_{3-x}Ti_4O_{12}$ systems. Figures 2 (a)–(c) show the Rietveld refinement of three $Ca_{1+x}Cu_{3-x}Ti_4O_{12}$ ceramic powders. The Rietveld refinement was performed through the GSAS (General Structure Analysis System) program.[32]

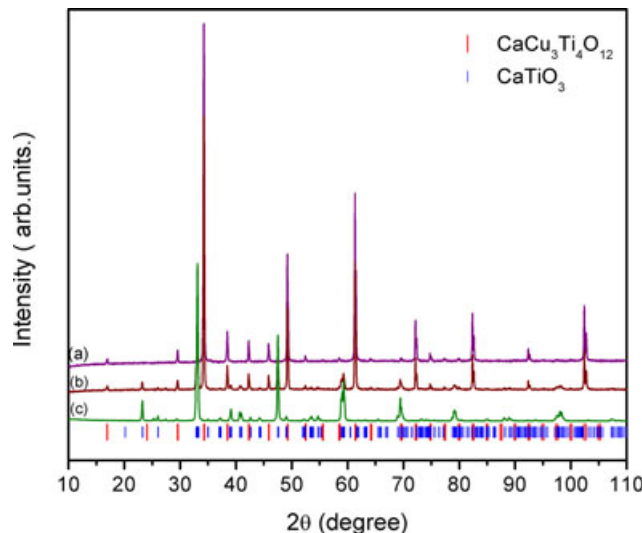**Fig. 1.** XRD patterns of CCTO($x = 0$) (a), CCTO/CTO($x = 1$) (b), and CTO($x = 3$) (c) powders prepared by the solid-state reaction.

The diffraction peak profiles were better adjusted by the Thompson-Cox-Hastings pseudo-Voigt (pV-TCH) function and by an asymmetry function as described by Finger et al.[33] The structural refinement results for CCTO($x = 0$), CCTO/CTO($x = 1$), and CTO($x = 3$) powders are listed in Table I.

The results in Table I show good agreement between observed XRD patterns and theoretical patterns. To evaluate the best fit, we used more than one criterion to judge the adequacy of the used model,[34,35] also shown in Table I: R_{WP}, R_{Bragg}, and χ^2. In the case of the CCTO($x = 0$) sample, good values are observed for R_{WP} and R_{Bragg}, but the χ^2 value is a little high. For the CCTO/CTO($x = 1$) system, R_{Bragg} value is not as good as the R_{WP} and χ^2 values. This behavior was expected since there are a mixture of phases ($CaCu_3Ti_4O_{12}$ and $CaTiO_3$) to be analyzed for the peak positions. By analyses of the CTO($x = 3$) sample, it can be observed that all R values obtained are good. These behaviors are in agreement with the $Y_{obs}-Y_{cal}$ as illustrated in Figs. 2(a)–(c). Figures 2(a) and (b) present a more difference in residual lines than Fig. 2(c). Moreover, the lattice parameter ($a = b = c = 7.397$) and average cell angles of $\alpha = \beta = \gamma = 90°$ estimated from the refinement confirmed a cubic structure for the $CaCu_{3-}Ti_4O_{12}$ phase. The lattice parameters ($a = 5.38$, $b = 5.44$, and $c = 7.64$) and average cell angles $\alpha = \beta = \gamma = 90°$ also confirmed an orthorhombic structure for the $CaTiO_3$ second phase. In Table I, the internal α^* and $\alpha^{\bullet}$ angle values observed for $CaCu_3Ti_4O_{12}$ and $CaTiO_3$, respectively, were obtained during the structural refinement in accordance with alterations in lattice parameters and internal positions values realized by the fitting during the refinement convergence.

The percentage of each phase in all systems studied is listed in Table I. The CCTO($x = 0$) system utilizes a monophasic (100% $CaCu_3Ti_4O_{12}$) as well as a CTO($x = 3$) (100% $CaTiO_3$) system. However, the CCTO/CTO($x = 1$) system contained 34.1% of a secondary phase. The Rietveld refinement results also show no significant changes in lattice parameters (a) ascribed to the $CaCu_3Ti_4O_{12}$ phase. In this system, the Cu atoms starts to occupy the Ca sites, resulting in a Ca-rich $CaCu_3Ti_4O_{12}$ solid solution, however, the solubility limit of Ca atoms in the system is low due to the difference of atomic radii between them. Thus, to obtain the $CaCu_3Ti_4O_{12}$ monophasic system, the Ca atomic fraction in the A site of the perovskite cannot exceed 25%, consequently, the excess of Ca in the CCTO/CTO($x = 1$) powder give rise to a $CaTiO_3$ secondary phase.[29] The as-formed two-phase $CaCu_3Ti_4O_{12}/CaTiO_3$ polycrystalline system has been considered a promising material due to its nonohmic and dielectric properties.[29–31]
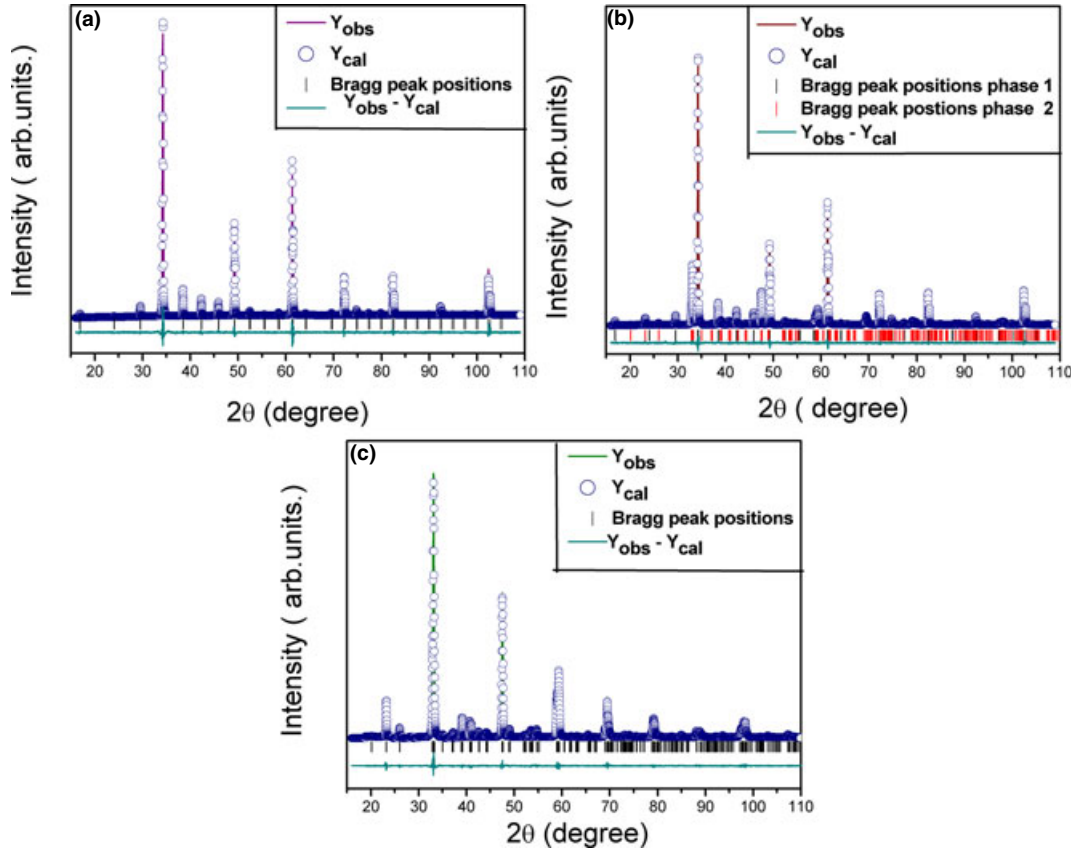
Fig. 2. Rietveld refinement data of CCTO($x = 0$) (a), CCTO/CTO($x = 1$) (b), and CTO($x = 3$) (c) powders prepared by the solid-state reaction; phase 1: $CaCu_3Ti_4O_{12}$ and phase 2: $CaTiO_3$.

Table I. Lattice Parameters, Percentage of Phases, $[TiO_6]$–α–$[TiO_6]$ Angle Values (α) for $Ca_{1+x}Cu_{3-x}Ti_4O_{12}$($x = 0$, 1.0, and 3.0) Powder Obtained by the Rietveld Refinement Method. Phase*: $CaCu_3Ti_4O_{12}$; Phase•: $CaTiO_3$

	Lattice parameters									
	a (Å)	b (Å)	c (Å)	Phase*	Phase•	α (°)*	α (°)•	R_B (%)	R_{wp} (%)	χ^2
CCTO($x = 0$)	7.397	7.397	7.397	100%		141.1		2.8	6.3	2.5
CCTO/CTO phase*	7.3971	7.3971	7.3971	65.9%		140.8		3.48	3.3	1.4
CCTO/CTO phase•	5.386	5.446	7.647		34.1%		158.4			
CTO($x = 3$)	5.384	5.442	7.644		100%		156.3	2.8	6.1	1.9

The crystalline structure of the $CaCu_3Ti_4O_{12}$ and $CaTiO_3$ phases is further well described in this article.

(2) Field Emission Scanning Electron Microscopy (FE-SEM)

Figures 3(a)–(f) present the FE-SEM images in BSE mode of the CCTO($x = 0$), CCTO/CTO($x = 1$), and CTO($x = 3$) systems prepared by the solid-state reaction. During the FE-SEM analyses, the EDXS analysis as well as the mapping of OK, CaK, TiK, and CuK elements in these samples, which are shown in Table II and Figs. 3(c), (f), and (i), respectively.

The images show that these systems are composed of several agglomerated particles with irregular morphologies, resulting in a nonuniform particle size distribution [Figs. 3 (a), (d), and (g)] arising from the ball milling stages in the solid-state reaction procedure. Moreover, in these systems, the loose particles are in contact by means of weak forces, including van der Waals forces. Thus, during the heat treatment, these newly formed contacts start sintering at the initial stage. As a consequence, the connectivity between the particles increases giving rise to a large aggregate of particles.

The CCTO system presents the majority of the particles in the range of 1.0–1.5 μm as well as the CCTO/CTO system.

The CCTO and CCTO/CTO powders are also heterogenous because of limited atomic diffusion of Ca, Cu, and Ti atoms through micrometer-sized grains. In the case of CCTO/CTO ($x = 1$), the heterogeneity is strongly dependent on the Ca/Cu ratio on this system, therefore, Cu-rich regions (Region 1) and Ca-rich regions (Region 2) is clearly seen in Fig.3(e). From this image, it was possible to observe the presence of some Cu atoms in Region 2, which are segregated in the particles surface. The obtained results are confirmed by the EDX analyses (Table II) and it can be seen from the CaK and CuK mapping [Fig. 3(f)], respectively. Moreover, they are in accordance with the Rietveld refinement analyses (Table I), where it was verified 65.9% of $CaCu_3Ti_4O_{12}$ and 34.1% of $CaTiO_3$ for this polycrystalline system were verified.

The CTO system presents particles in the range of 500 nm –2.0 μm. Moreover, the mapping of CaK, TiK, and OK elements also indicates that this sample is homogeneous in its composition.

(3) Representation of $CaCu_3Ti_4O_{12}$ and $CaTiO_3$ Unit Cell: Structural Defects

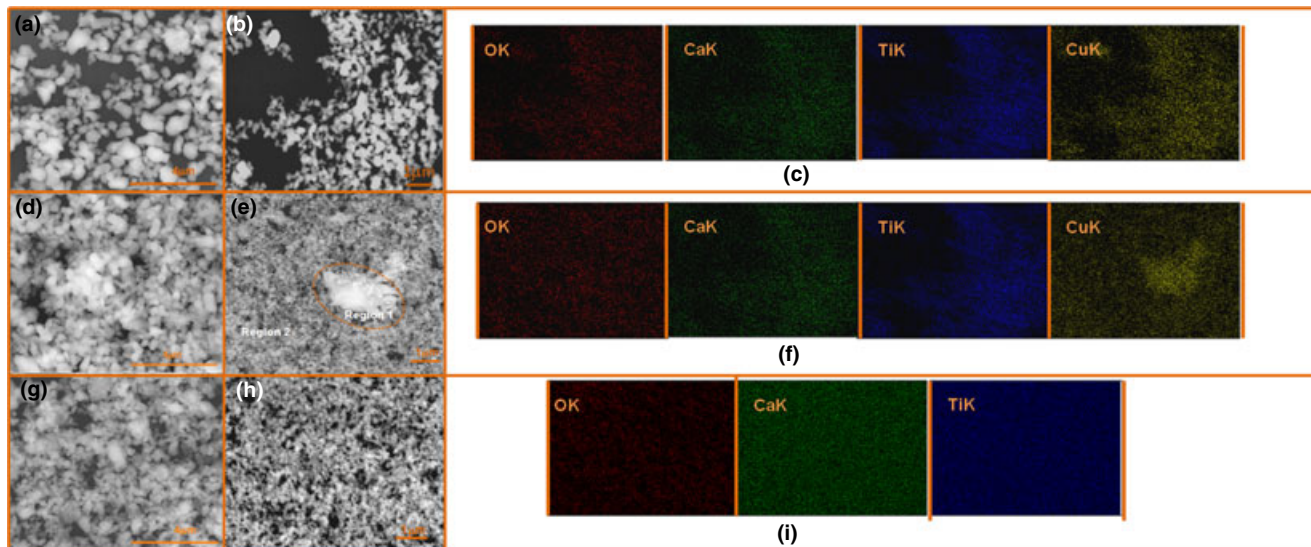Figures 4(a) and (b) show a schematic representation of $CaCu_3Ti_4O_{12}$ and $CaTiO_3$ unit cells modeled through the

Fig. 3. FE-SEM images of the CCTO($x = 0$) (a, b), CCTO/CTO($x = 1$) (d, e), CTO($x = 3$) (g, h) systems, respectively. Mapping of the OK, CaK, TiK, and CuK elements of CCTO (c), CCTO/CTO (f), and CTO (i) systems.

Table II.   Percentage of Elements Presents in CCTO($x = 0$), CCTO/CTO($x = 1$), and CTO($x = 3$) Powders Obtained by Means of EDXS Analysis

Elements	CCTO	CCTO/CTO region 1	CCTO/CTO region 2	CTO
CaK	3.42	4.01	5.56	23.28
CuK	11.11	15.79	4.82	
TiK	14.28	7.48	10.11	24.24
OK	71.20	35.93	34.23	52.47

Diamond-Crystal and Molecular Structure Visualization software (DEMO version for Windows).[36] Atomic coordinates obtained from the Rietveld refinement (Table I) were used to model the structures.

$CaCu_3Ti_4O_{12}$ material has a body-centered cubic structure with a space group *Im-3*. In this structure, one-fourth of A sites are occupied by Ca and three-fourth of these sites are occupied by Cu atoms.[37] The Ca atoms are coordinated with 12 oxygen atoms which form $[CaO_{12}]$ clusters in a cuboctahedral configuration. The Cu atoms are coordinated with four oxygen atoms which form $[CuO_4]$ clusters in a square planar configuration as a result of the Jahn-Teller effect.[38,39] Ti atoms are located at B sites which are coordinated with six oxygen atoms in an octahedral configuration. These $[TiO_6]$ octahedra are displaced from the symmetric center to accommodate $[CuO_4]$ clusters in the $CaCu_3Ti_4O_{12}$ cubic structure.[40,41] On the other hand, these $[CuO_4]$ and $[TiO_6]$ clusters are bonded to each other with $[TiO_6]$-α-$[TiO_6]$ angles of ~141°($x = 1.0$). Such a variation is also controlled by the oxygen position of 1.971 and 1.966 Å in the $Ca_{1+x}Cu_{3-x}Ti_4O_{12}$ system ($x = 0.0$ and 1.0) [see Fig. 4(a)].

In recent years, several articles were published which propose a structural model for the $CaCu_3Ti_4O_{12}$ material.[10,42] Different techniques such as transmission electron microscopy (TEM)[42] and electron paramagnetic resonance (EPR)[43] confirmed polaron defects at twinned nanodomains. According to these authors, distortions in $[TiO_6]$ clusters caused by changes in the bond length of Cu–O could increase the number of clusters $[TiO_5V_O^{\bullet}]$-$[TiO_6]$ in the structure [see Fig. 4(a)]. In this case, the conductivity of the CCTO would occur by charge transference from $[TiO_5V_O^{\bullet}]$ to $[CuO_4]'$ and from $[TiO_5V_O^{x}]$ to $[CuO_4]^x$ or $[CuO_4]'$ to $[CuO_4]^x$ clusters. Moreover, this process gives rise to Cu^+ species ($[CuO_4]'$) in the lattice. In this process, there is movement of electrons
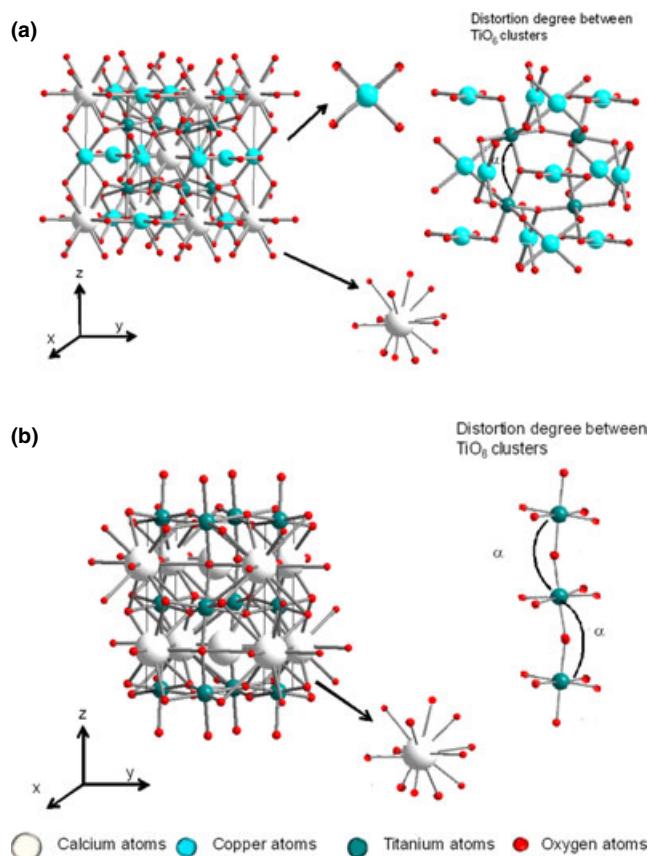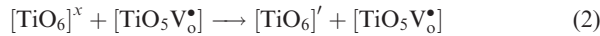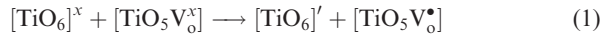

Fig. 4. Schematic representation of a $CaCu_3Ti_4O_{12}$ unit cell (a) and $CaTiO_3$ unit cell (b).

into $3d$ orbitals of Ti atoms, forming Ti^{3+} cations, which works as charge carriers in the material. According to some authors, the presence of this species can also be influenced by the copper content into $CaCu_3Ti_4O_{12}$ system. In this case, the origin of these species is from the reduction of CuO during the sintering process.[41–46] These species play an important role in the formation of hole-electron ($h^{\bullet}$-e^-) pairs which results in a charge gradient in the lattice.
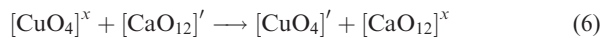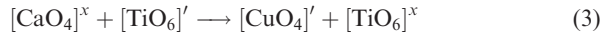
Another point to consider is the existence of $[CaO_{12}V_O^z]$ clusters in the $CaCu_3Ti_4O_{12}$ structure. In this case, the

charge transfer process will occur from $[TiO_5V_o^\bullet]$ to $[TiO_6]'$ or from $[CaO_{11}V_o^\bullet]$ to $[CaO_{12}]'$. To understand this phenomenon, the Kröger–Vink notation[47] was used to describe the electronic charge of the cationic species in the $CaCu_3Ti_4O_{12}$ system. Thus, the complex oxygen vacancies $(V_o^x, V_o^\bullet, \text{and } V_o^{\bullet\bullet})$ stabilized the lattice defects via charge compensation.

For the network formers:

$$[TiO_6]^x + [TiO_5V_o^x] \longrightarrow [TiO_6]' + [TiO_5V_o^\bullet] \qquad (1)$$

$$[TiO_6]^x + [TiO_5V_o^\bullet] \longrightarrow [TiO_6]' + [TiO_5V_o^\bullet] \qquad (2)$$

Also, this model can be extended for the network modifiers:

$$[CaO_4]^x + [TiO_6]' \longrightarrow [CuO_4]' + [TiO_6]^x \qquad (3)$$

$$[CaO_{12}]^x + [CaO_{11}V_o^x] \longrightarrow [CaO_{12}]' + [CaO_{11}V_o^\bullet] \qquad (4)$$

$$[CuO_{12}]^x + [CaO_{11}V_o^\bullet] \longrightarrow [CaO_{12}]' + [CaO_{11}V_o^{\bullet\bullet}] \qquad (5)$$

$$[CuO_4]^x + [CaO_{12}]' \longrightarrow [CuO_4]' + [CaO_{12}]^x \qquad (6)$$

$$[CuO_4]' \xrightarrow{e'} [CuO_4]^x \text{ where, } Cu^{II} \text{ and } Cu^{I} \qquad (7)$$

In the $CaTiO_3$ structure, Ca atoms are coordinated to 12 oxygens atoms, and the Ti is coordinated to six oxygens atoms ($[CaO_{12}]$ and $[TiO_6]$ clusters). The adjacent $[TiO_6]$ clusters are also displaced from the symmetric center [see Fig. 4(b)] and show angles between $[TiO_6]$–α–$[TiO_6]$ clusters of ~156°(CTO) and 158°(CCTO:Ca) (see Table I). These changes in α angles in the $CaTiO_3$ phase are strongly related to the formation of $[TiO_6]_d^\bullet \leftrightarrow [TiO_6]_o'$ clusters (o = ordered, d = disordered).[48] Thus, the distortion between these complex clusters causes a polarization and/or a difference in the charge density in the orthorhombic structure[49] which is able to promote a charge transfer from the $[TiO_6]_d^x$ to the $[TiO_6]_o^x$. These complex clusters can also create hole (h$^\bullet$)-electron (e$^-$)-polarons in the CTO as well as in CCTO/CTO(x = 1.0) systems which potentially influence its optical properties.[50] The charge transference in the Ca-TiO_3 phase is also represented by the Kröger–Vink notation in Eq. (8).

For the $CaTiO_3$ lattice former:

$$[TiO_6]_o^x + [TiO_6]_d^x \longrightarrow [TiO_6]_o' + [TiO_6]_d^\bullet \qquad (8)$$
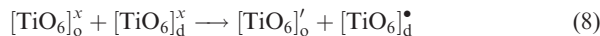
Also, the proposed model for the lattice former can be extended for the network modifiers and is represented by Eq. (9):

$$[CaO_{12}]_o^x + [CaO_{12}]_d^x \longrightarrow [CaO_{12}]_o' + [CaO_{12}]_d^\bullet \qquad (9)$$

In this work, we propose that the charge transference is responsible for the PL response of $CaCu_3Ti_4O_{12}$ and $CaTiO_3$ structures as a consequence of different structural defects. The $CaCu_3Ti_4O_{12}$ could be mainly associated with oxygen vacancies ($[TiO_5V_o^\bullet]$, $[TiO_5V_o^{\bullet\bullet}]$, $[CaO_{11}V_o^\bullet]$, $[CaO_{11}V_o^{\bullet\bullet}]$). On the other hand, the optical properties of the $CaTiO_3$ structure possibly arises from distortions/strains in the ($[TiO_6]_d^\bullet \leftrightarrow [TiO_6]_o'$ complex and $[CaO_{12}]_d^\bullet \leftrightarrow [CaO_{12}]_o'$).

(4) XANES Analyses

Figures 5(a)–(d) show Ti K-edge XANES spectra of CCTO (x = 0), CCTO/CTO (x = 1), and CTO(x = 3) powders.
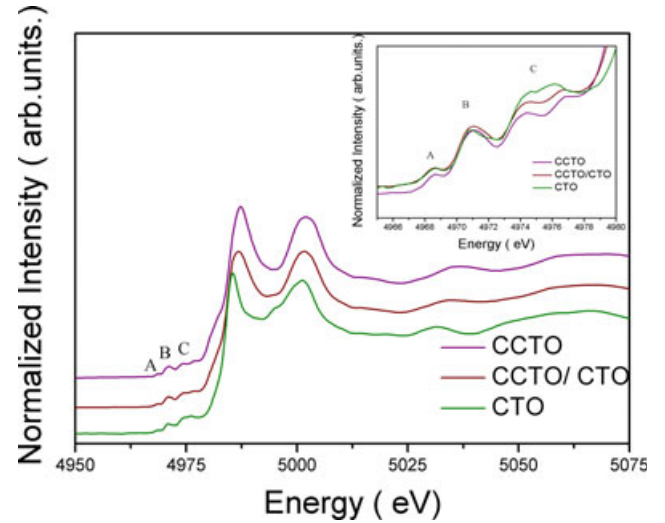
Fig. 5. (a) Ti K-edge XANES spectra of CCTO(x = 0), CCTO/CTO(x = 1), and CTO(x = 3) powders. Inset of the expanded view of the pre-edge region of normalized XANES spectra for CCTO (x = 0), CCTO/CTO(x = 1), and CTO(x = 3) samples.

The XANES region is comprised in the range of 50 eV above the absorption region of the analyzed material. In case of Ti atoms, the XANES region is comprised at 4966 eV.[51] The inset of Fig. 5 shows that the pre-edge region is composed of three peaks at 4968 (a), 4971 (b), and 4975 eV (c), respectively. The A peak is caused by a quadrupole excitation from the 1s electron to the t_{2g} orbitals of the absorbing $[TiO_6]$ octahedral. The B peak arises from the excitation of the 1s electron to the e_g orbitals of its octahedra which is caused by p-d mixing contributions. Finally, the feature of C peak in the pre-edge region is attributed to dipole excitations of Ti 1s electrons into e_g orbitals of neighboring $[TiO_6]$ octahedra.[52–54]

The XANES analysis was employed in several theoretical studies of structurally disordered titanates reported by our research group. The research indicated that the area and intensity of the pre-edge B peak can provide information about complex clusters $[TiO_5]$ and $[TiO_6]$ as well as the local environment of Ti in the titanate structures.[54,55] Figure 4 illustrates the characteristic pre-edge peak observed for $Ca_{1+x}Cu_{3-x}Ti_4O_{12}$ systems (x = 0.0, 1.0, and 3.0) which is characteristic of a five-coordination of $[TiO_5]$ clusters and a six-coordination of octahedral $[TiO_6]$ clusters. In addition, the higher intensity of this peak indicates that the local environment of Ti is noncentrosymmetric; i.e., distorted from its symmetric center.[48, 50]

To estimate the percentage of $[TiO_5]$ and $[TiO_6]$ complex clusters in $Ca_{1+x}Cu_{3-x}Ti_4O_{12}$ systems (see Fig. 6), each B peak area (located at around 4971 eV) was evaluated. Figure 6 shows that the XANES analysis for CCTO(x = 0) powder indicated a higher percentage (98%) of Ti fivefold coordination ($[TiO_5V_o^z]$) which is associated with oxygen vacancies ($V_o^z = V_o^x$, $V_o^\bullet$, and $V_o^{\bullet\bullet}$) between the clusters $[TiO_6\text{-}TiO_5.V_o^z]$ in the $CaCu_3Ti_4O_{12}$ structure.[56,57]

To facilitate a better analysis of the Ti-K XANES spectrum of the CCTO/CTO (x = 1) system (see Fig.6), it was necessary to perform a linear combination of CCTO(x = 0) and CTO(x = 3) XANES spectra using the appropriate amount estimated for each phase through the Rietveld refinement method (see Table I). Using the analysis of the pre-edge region for this powder, the Ti-K XANES spectrum for the CCTO/CTO(x = 1) system can be described by the contribution of $CaCu_3Ti_4O_{12}$ and $CaTiO_3$ crystalline phases. The increase in the intensity of the C peak compared to the CCTO(x = 0) powder (see inset of Fig. 5) is mainly ascribed to the covalent nature of Cu-O in the $CaCu_3Ti_4O_{12}$ structure. This phenomenon is responsible for the appearance of $[TiO_{5-}$
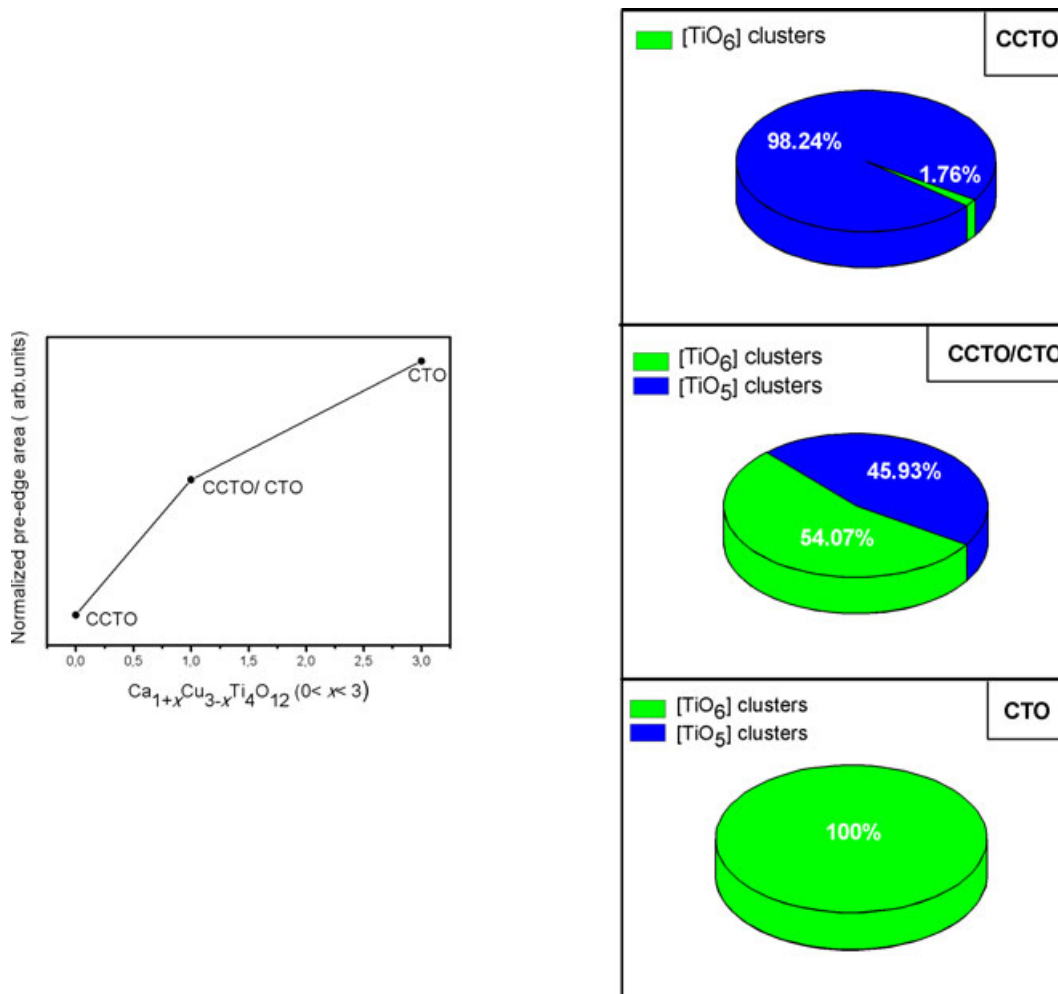
Fig. 6. Calculated area by means of integration of XANES spectra in the range from 4960 to 4990 eV for CCTO($x = 0$), CCTO/CTO($x = 1$), and CTO($x = 3$) powders and percentages for [TiO$_5$] and [TiO$_6$] clusters presented in these systems.

V_O^z]-[TiO$_6$] in the structure. Moreover, it is verified 47% of [TiO$_5$] and 54% of [TiO$_6$] clusters (distorted [TiO$_6$] octa hedrons) in the CCTO/CTO($x = 1$) system. These results suggest that the structural defects of CaCu$_3$Ti$_4$O$_{12}$ and CaTiO$_3$ structures can influence the charge transference as well as optical properties of this system.

From the XANES analysis of the CTO powders, the increase in the area of the pre-edge B peak compared to the CCTO system suggests an increase in the concentration of Ti sixfold coordination (distorted [TiO$_6$] octahedrons) and the number of $[TiO_6]_d^\bullet \leftrightarrow [TiO_6]_o'$ cluster species in the system. All results obtained are in agreement with the proposed structural model presented in this report.

(5) UV–vis Absorption Spectroscopy Analyses

UV–vis absorbance spectra for Ca$_{1+x}$Cu$_{3-x}$Ti$_4$O$_{12}$ systems are presented in Figs. 7(a)–(d), respectively. Wood and Tauc[58] demonstrated a relationship between the absorption curve and the energy gap of the material. Band gap values are obtained by extrapolating the linear region of the curve. According to this method, the energy dependence of the gap and the optical absorbance follows Eq. (10).

$$h v \alpha \propto (h v - E_{gap}^t)^2 \qquad (10)$$

where α is the absorbance, h is the Planck's constant, v is the frequency, and E_{gap}^t is the band gap of the material where the t constant is associated with different types of electronic transitions ($t = 1/2$, 2, 3/2, or 3 for direct allowed, indirect allowed, direct forbidden, and indirect forbidden transitions,

respectively). In this report, optical band gap values are listed in Figs. 7(a)–(d).

The electronic transitions of CaCu$_3$Ti$_4$O$_{12}$ powders are ascribed to charge electronic transitions between the $2p$ orbitals of oxygen atoms in the valence band (VB) and $3d$ orbitals of copper atoms in the conduction band (CB). Fahan *et al.*[59] studied the electronic properties of CaCu$_{3-}$Ti$_4$O$_{12}$ by means of *ab initio* calculations, based on spin-polarized density-functional theory. The electronic band structure indicated electronic transitions from the maximum-energy states (near or inside), the VB to minimum-energy states (below or inside), the CB, in a different regions in the Brillouin zone (indirect band gap). Moreover, we obtained a direct band gap value of 0.24 eV and an indirect band gap of 0.18 eV. The difference between these two values is lower due to the conductive character presented by this powder. In this article, the experimental band gap value was evaluated as 1.5 eV. The literature also reported experimental band gap values in the range of 2.0–3.5 eV.[60,61]

The calculated band structures [48,54,55,62] also showed that the electronic transition for CaTiO$_3$ powders occurs inside [TiO$_6$] octahedral clusters since $2p$ orbitals of oxygen atoms in VB and $3d$ orbitals of the titanium atoms can be associated with the CB [see Fig. 6(c)]. These electronic states can be perturbed or nonuniformly distributed in the Brillouin zone. Thus, for Ca$_{1+x}$Cu$_{3-x}$Ti$_4$O$_{12}$ powders prepared by the solid-state reaction, interactions that influence E_{gap} values are related to copper in the CaCu$_3$Ti$_4$O$_{12}$ system and to distortions or strains associated with [TiO$_6$] clusters in the CaTiO$_3$ lattice.

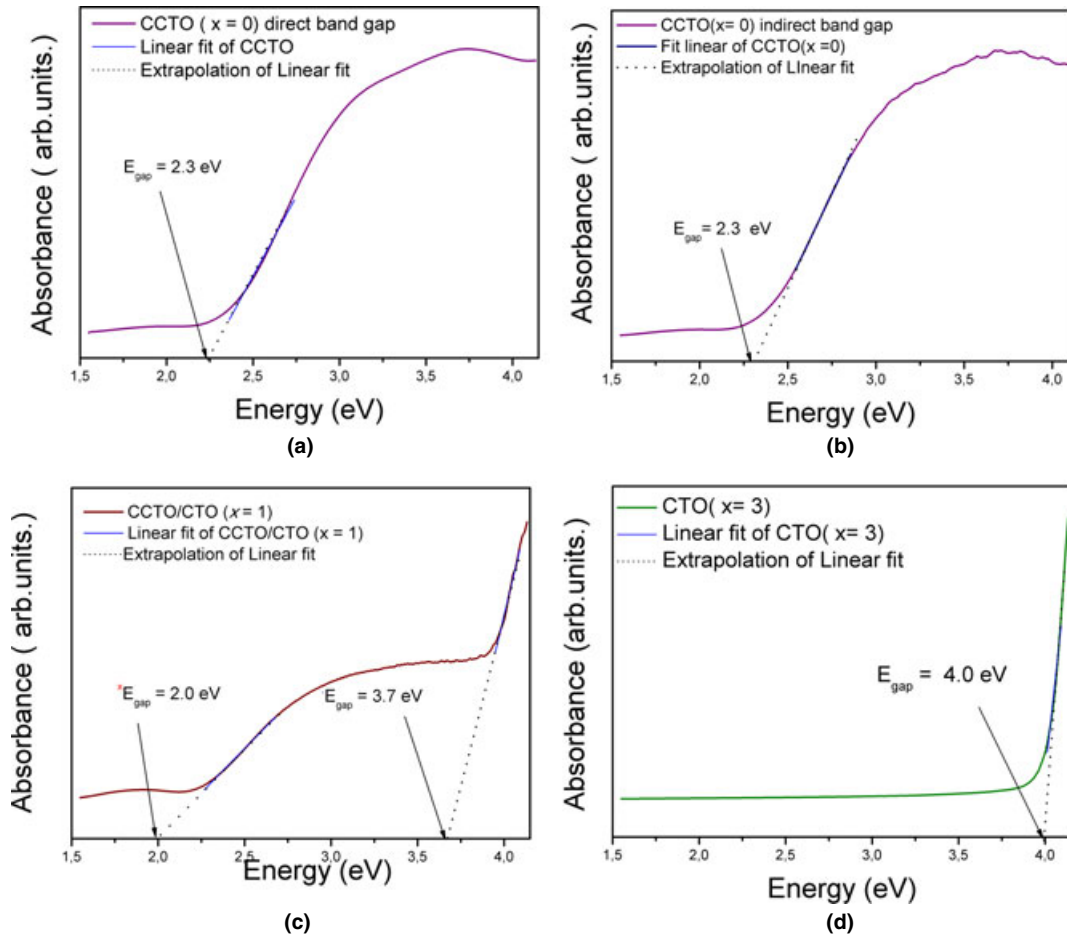**Fig. 7.** UV–vis absorbance spectra of CCTO($x = 0$) (a and b), CCTO/CTO($x = 1$) (c), and CTO (d) systems (*$CaCu_3Ti_4O_{12}$ and ·$CaTiO_3$).

In this present work, the band structure for $CaCu_3Ti_4O_{12}$ was considered a direct transition and an indirect for the CCTO($x = 0$) system. Therefore, the value of $n = 0.5$ and $n = 2.0$ were used for direct and indirect band gap in Eq. (9), respectively. From Figs. 7(a) and (b), we found the same band gap value of 2.3 eV for both electronic transitions.

As there is no difference between the direct and indirect band gap for CCTO($x = 0$) system, we consider a direct transition for the CCTO/CTO system, because of the $CaTiO_3$ secondary phase, which presents a direct transition. The CCTO/CTO($x = 1.0$) powder shows two band gap values [see Fig. 7(c)] associated with the $CaCu_3Ti_4O_{12}$ (2.0 eV) phase and the $CaTiO_3$ phase (3.7 eV). The segregation of the $CaTiO_3$ secondary phase leads to a lower contribution from $3d$ orbitals of Cu and a higher contribution from Ti $3d$ orbitals of the $CaTiO_3$ which confirms that both phases can contribute to the appearance of energetic levels between the valence and CB.

For the CTO system, a band gap value of 4.0 eV was produced as a result of structural defects (mostly distortions and/or strains in the $CaTiO_3$ structure). In the CTO system, these defects are able to induce a symmetry break of $[TiO_6]$ and $[CaO_{12}]$ which leads to an additional contribution of $3d$ Ti electronic levels to compose energetic levels between valence and CB.

(6) PL Measurements

For a better understanding of PL properties and their dependence on the structural order–disorder in ceramic powders, PL emission spectra of $Ca_{1+x}Cu_{3-x}Ti_4O_{12}$ systems were taken. Emission spectra were taken at room temperature; the broad emission band with a maximum situated at 440 nm was also observed.
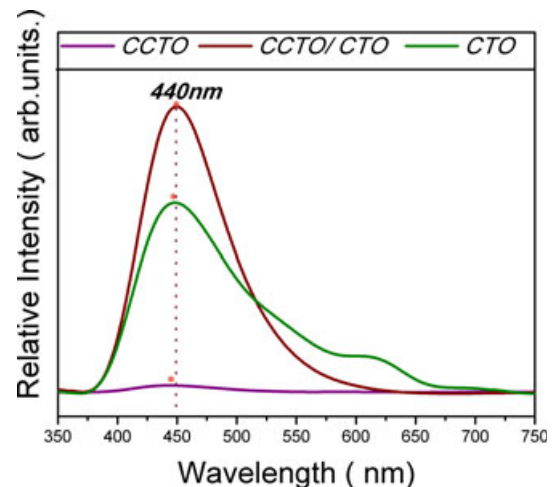

Fig. 8. PL emission spectra of CCTO($x = 0$), CCTO/CTO($x = 1$), and CTO($x = 3$) powders prepared by the solid-state reaction.

The CCTO system has a lower PL emission intensity (see Fig. 8). UV–vis spectra for this sample [see Fig. 7(a)] reveal that the concentration of copper is strongly related to the conductive character of the powder (2.3 eV).[51]

However, with excess Ca, $CaTiO_3$ induced an additional contribution of $3d$ Ti electronic levels in electronic states which can be associated with the PL intensity enhancement as x increases from 0 to 1.0. For the CCTO/CTO($x = 1.0$) system, we believe that the PL intensity is strongly related to the difference in the charge process transference. The charge density in the $CaCu_3Ti_4O_{12}$ phase produces a more favorable

charge transference process from the $[CuO_4]'$ to $[CuO_4]^x$, and from the $[TiO_6]^x_d$ to $[TiO_6]^x_o$, or $[CaO_{11}V_o^x]$ to $[CaO_{12}]^x$ [see Eqs. (1)–(7)]. In the CaTiO$_3$ phase, as a consequence of the excess Ca, the charge density could arise from the breaking symmetry of $[CaO_{12}]$ and $[TiO_6]$ clusters caused by distortions/strains in the lattice which thus produces a more favorable charge transference process from the $[TiO_6]^x_d \xrightarrow{e'} [TiO_6]^x_o$ and $[CaO_{12}]^x_d \xrightarrow{e'} [CaO_{12}]^x_o$.

Figure 8 illustrates that CTO powder causes a decrease in the PL intensity. In this system, electronic energy states will be composed mainly of the oxygen $2p$ (VB) and titanium $3d$ (CB) which results in an increase in the energy gap value; i.e., a reduction in intermediate levels of energy. Otherwise, this increase is not related to a structural organization but is a contribution of different types of orbitals. Another point to consider for this system is the formation of structural defects such as distortions or strains which create $[TiO_6]^\bullet_d \leftrightarrow [TiO_6]'_o$ clusters in the CaTiO$_3$ lattice and charge transference between these clusters.

IV. Conclusions

From the results obtained, the CaCu$_3$Ti$_4$O$_{12}$ cubic structure (*Im-3*) and CaTiO$_3$ orthorhombic (*Pbnm*) phases in the systems were verified. Rietveld refinements indicate that excess Ca atoms added to the CCTO/CTO($x = 1.0$) segregated in a CaTiO$_3$ secondary phase which suggests that solubility limit of Ca atoms in the CaCu$_3$Ti$_4$O$_{12}$ lattice was reached for this system. The FE-SEM images show that the Ca$_{1+x}$Cu$_{3-x}$Ti$_4$O$_{12}$ $(0 < x < 3)$ powders are composed of several agglomerated particles with irregular morphology. The CCTO($x = 0$) and CCTO/CTO($x = 1$) systems are compositional and heterogeneous. This behavior was attributed to the limited atomic diffusion of Ca, Cu, and Ti atoms through micrometer-sized grains. Moreover, a Cu-rich region and a Ca-rich region was noticed for the CCTO/CTO($x = 1$) polycrystalline system, which was confirmed by EDXS analyses. XANES spectra indicate that structural defects associated with oxygen vacancies ($[TiO_6–TiO_5.V_o^z]$) could be present in the CaCu$_3$Ti$_4$O$_{12}$ structure and distorted $[TiO_6]$ in the CaTiO$_3$ structure. UV–vis absorbance spectra indicate an increase in E_{gap} values. The CCTO/CTO $(x = 1.0)$ system has two E_{gap} values which are associated with CaCu$_3$Ti$_4$O$_{12}$ and CaTiO$_3$ phases. This behavior is associated with an additional contribution of $3d$ Ti electronic levels of CaTiO$_3$. Ca$_{1-x}$Cu$_{3-x}$Ti$_4$O$_{12}$ ($x = 0.0$, 1.0, and 3.0) systems presented a PL emission at 440 nm where the intensity is probably related to structural defects in CaCu$_3$Ti$_4$O$_{12}$ (oxygen vacancies) and CaTiO$_3$ (distortions/strains) phases and potentially influence the charge transference process as well as its optical properties.

References

[1]W. K. Chen, C. M. Cheng, J. Y. Huang, W. F. Hsieh, and T. Y. Tseng, "Study of Linear and Nonlinear Optical Properties of Distorted Ti–O$_6$ Perovskite Structure in BaxSr$_{1-x}$TiO$_3$," *J. Phys. Chem. Sol.*, **61**, 969–77 (2000).

[2]M. A. Subramanian, D. Li, N. Duan, B. A. Reisner, and A. W. Sleight, "High Dielectric Constant in ACu$_3$Ti$_4$O$_{12}$ and ACu$_3$Ti$_3$FeO$_{12}$ Phases," *J. Solid State Chem.*, **151** [2] 323–5 (2000).

[3]D. C. Sinclair, T. B. Adams, F. D. Morrison, and A. R. West, "CaCu$_3$Ti$_4$O$_{12}$: Onestep Internal Barrier Layer Capacitor," *Appl. Phys. Lett.*, **80** [12] 2153–5 (2002).

[4]A. P. Ramirez, M. A. Subramanian, M. Gardel, G. Blumberg, D. Li, T. Vogt, and S. M. Shapiro, "Giant Dielectric Constant Response in a Copper-Titanate," *Solid State Comm.*, **115**, 217–20 (2000).

[5]C. C. Homes, T. Vogt, S. M. Shapiro, S. Wakimoto, A. P. Ramirez, "Optical High-Dieletric Constant Perovskite Related Oxide," *Science*, **293**, 673–6 (2001).

[6]T. T. Fang and C. P. Liu, "Evidence of the Internal Domains for Inducing the Anomalously High Dielectric Constant of CaCu$_3$Ti$_4$O$_{12}$," *Chem. Matter.*, **17**, 5167–71 (2005).

[7]M. H. Cohen, J. B. Neaton, L. X. He, and D. Vanderbilt, "Extrinsic Models for the Dielectric Response of CaCu$_3$Ti$_4$O$_{12}$," *J. Appl. Phys.*, **94**, 3299–306 (2003).

[8]C. C. Wang and L. W. Zhang, "Surface-Layer Effect in CaCu$_3$Ti$_4$O$_{12}$," *Appl. Phys. Lett.*, **88**, 042906, 3pp (2006).

[9]I. D. Kim, A. Rothschild, and H. L. Tuller, "Direct Current Bias Effects on Grain Boundary Schottky Barriers in CaCu$_3$Ti$_4$O$_{12}$," *Appl. Phys. Lett.*, **88**, 072902, 3pp (2006).

[10]P. R. Bueno, R. Tararam, R. Parra, E. Joanni, M. A. Ramirez, W. C. Ribeiro, E. Longo, and J. A. Varela, "A Polaronic Stacking Fault Defect Model for CaCu$_3$Ti$_4$O$_{12}$ Material: an Approach for the Origin of the Huge Dielectric Constant and Semiconducting Coexistent Features," *J.Phys. D: Appl. Phys.*, **42**, 055404, 9pp (2009).

[11]S. Y. Chung, I. D. Kim, and S. J. L. Kang, "Strong Nonlinear Current-Voltage Behaviour in Perovskite-Derivative Calcium Copper Titanate," *Nat. Mater.*, **3**, 774–8 (2004).

[12]C. H. Mu, P. Liu, Y. He, J. P. Zhou, and H. W. Zhang, "An Effective Method to Decrease Dielectric Loss of CaCu$_3$Ti$_4$O$_{12}$ Ceramics," *J. Alloy. Compd.*, **471** [1–2] 137–41 (2009).

[13]D. R. Clarke, "Varistors Ceramics," *J. Am. Ceram. Soc.*, **82**, 485–502 (1999).

[14]L. Feng, X. Tang, Y. Yan, X. Chen, Z. Jiao, and G. Cao, "Decrease of Dielectric Loss in CaCu$_3$Ti$_4$O$_{12}$ Ceramics by La Doping," *Phys. Status Solidi A*, **203** [4] R22–4 (2006).

[15]A. Sen, U. N. Maiti, R. Thapa, and K. K. Chattopadhyay, "Effect of Vanadium Doping on the Dielectric and Nonlinear Current–Voltage Characteristics of CaCu$_3$Ti$_4$O$_{12}$ Ceramic," *J. Alloy. Compd.*, **506** [2] 853–7 (2010).

[16]R. Schmidt and D. C. Sinclair, "Anomalous Increase of Dielectric Permittivity in Sr-Doped CCTO Ceramics Ca$_{1-x}$Sr$_x$Cu$_3$Ti$_4$O$_{12}$ ($0 \leq x \leq 0.2$)," *Chem. Mater.*, **22** [1] 6–8 (2010).

[17]M. Li, G. Cai, D. F. Zhang, W. Y. Wang, W. J. Wang, and X. L. Chen, "Enhanced Dielectric Responses in Mg-Doped CaCu$_3$Ti$_4$O$_{12}$," *J. Appl. Phys.*, **104** [7] 074107, 4pp (2008).

[18]T. Li, Z. P. Chen, F. G. Chang, J. H. Hao, and J. C. Zhang, "The Effect of Eu$_2$O$_3$ Doping on CaCu$_3$Ti$_4$O$_{12}$ Varistor Properties," *J. Alloy. Compd.*, **484** [1–2] 718–22 (2009).

[19]S. D. Hutagalung, L. Y. Ooi, and Z. A. Ahmad, "Improvement in Dielectric Properties of Zn-Doped CaCu$_3$Ti$_4$O$_{12}$ Electroceramics Prepared by Modified Mechanical Alloying Technique," *J. Alloy. Compd.*, **476** [1–2] 477–81 (2009).

[20]E. A. Patterson, S. Kwon, C. C. Huang, and D. P. Cann, "Effects of ZrO$_2$ Additions on the Dielectric Properties of CaCu$_3$Ti$_4$O$_{12}$," *Appl. Phys. Lett.*, **87** [18] 182911, 3pp (2005).

[21]Y. H. Lin, J. N. Cai, M. Li, C. W. Nan, and J. L. He, "Grain Boundary Behavior in Varistor-Capacitor TiO$_2$-Rich CaCu$_3$Ti$_4$O$_{12}$ Ceramics," *J. Appl. Phys.*, **103** 074111, 5pp (2008).

[22]S. D. Hutagalung, M. I. M. Ibrahim, and Z. A. Ahmad, "The Role of Tin Oxide Addition on the Properties of Microwave Treated CaCu$_3$Ti$_4$O$_{12}$," *Mater. Chem. Phys.*, **112** [1] 83–7 (2008).

[23]T. Li, K. Fang, J. Hao, Y. Xue, and Z. Chen, "The Effect of Ca-Rich on the Electric Properties of Ca$_{1+x}$Cu$_{3-x}$Ti$_4$O$_{12}$ Polycrystalline System," *Mat. Sci. Eng. B: Solid State Mat. Adv. Technol.*, **176** [2] 171–6 (2011).

[24]R. Parra, R. Savu, L. A. Ramajo, M. A. Ponce, J. A. Varela, M. S. Castro, P. R. Bueno, and E. Joanni, "Sol–Gel Synthesis of Mesoporous CaCu$_3$Ti$_4$O$_{12}$ Thin Films and Their Gas Sensing Response," *J. Solid State Chem.*, **183** [6] 1209–14 (2010).

[25]R. Parra, E. Joanni, J. W. M. Espinosa, R. Tararam, M. Cilense, P. R. Bueno, J. A. Varela, and E. Longo, "Photoluminescent CaCu$_3$Ti$_4$O$_{12}$-Based Thin Films Synthesized by a Sol–Gel Method," *J. Am. Ceram. Soc.*, **91** [12] 4162–4 (2008).

[26]V. M. Longo, L. S. Cavalcante, R. Erlo, V. R. Mastelaro, A. T. de Figueiredo, J. R. Sambrano, S. de Lazaro, A. Z. Freitas, L. Gomes, N. D. Vieira, J. A. Varela, and E. Longo, "Strong Violet–Blue Light Photoluminescence Emission at Room Temperature in SrZrO$_3$: Joint Experimental and Theoretical Study," *Acta Mater.*, **56** [10] 2191–202 (2008).

[27]B. Ravel and M. Newville, "ATHENA and ARTEMIS: Interactive Graphical Data Analysis Using IFEFFIT," *Phys. Scr.*, **T115**, 1007–10 (2005).

[28]B. Ravel and M. Newville, "ATHENA, ARTEMIS, HEPHAESTUS: Data Analysis for X-Ray Absorption Spectroscopy using IFEFFIT," *J. Synchrot. Radiat.*, **12**, 537–41 (2005).

[29]M. A. Ramirez, P. R. Bueno, J. A. Varela, and E. Longo, "Non-Ohmic and Dielectric Properties of aCa$_2$Cu$_2$Ti$_4$O$_{12}$ Polycrystalline System," *Appl. Phys. Lett.*, **89** [21] 212102, 3pp (2006).

[30]M. A. Ramirez, P. R. Bueno, E. Longo, and J. A. Varela, "Conventional and Microwave Sintering of CaCu$_3$Ti$_4$O$_{12}$/CaTiO$_3$ Ceramic Composites: Non-Ohmic and Dielectric Properties," *J. Phys. D: Appl. Phys.*, **41** [15] 152004, 6pp (2008).

[31]P. R. Bueno, W. C. Ribeiro, M. A. Ramirez, J. A. Varela, and E. Longo, "Separation of Dielectric and Space Charge Polarizations in CaCu$_3$Ti$_4$O$_{12}$/CaTiO$_3$ Composite Polycrystalline Systems," *Appl. Phys. Lett.*, **90** 055404, 3pp (2007).

[32]A. C. Larson and R. B. Von Dreele, "General Structure Analysis System"; Los Alamos National Laboratory Report No. LAUR, 86, 2004.

[33]L. W. Finger, D. E. Cox, and A. P. Jephcoat, "A Correction for Powder Diffraction Peak Asymmetry Due to Axial Divergence," *J. Appl. Crystallogr.*, **27** [6] 892–900 (1994).

[34]E. Jansen, W. Schäfer, and G. Will, "R Values in Analysis of Powder Diffraction Data Using Rietveld Refinement," *J. Appl. Phys.*, **27**, 492–6 (1994).

[35]M. Sakata and M. J. Cooper, "An Analysis of the Rietveld Profile Refinement Method," *J. Appl. Cryst.*, **12** 554–63 (1979).

[36]H. Putz and K. Brandenburg, *Crystal Impact-Software for Chemists and Materials Science*. Germany, 1997–2012.

[37]K. S. Aleksandrov and B. V. Beznosikov, "Crystal Chemistry and Prediction of Compounds with a Structure of Skutterudite Type," *Crystallogr. Rep.*, **52**, 28–36 (2007).

[38]S. M. Moussa and B. J. Kennedy, "Structural Studies of the Distorted Perovskite $Ca_{0.25}Cu_{0.75}TiO_3$," *Mater. Res. Bull.*, **36** [13–14] 2525–9 (2001).

[39]A. N. Vasil'ev and O. S. Volkova, "New Functional Materials AC(3)B(4) O(12) (Review)," *J. Low Temp. Phys.*, **33** [11] 895–914 (2007).

[40]U. Schwingenschlogl, V. Eyert, and U. Eckern, "Octahedral Tilting in $ACu_3Ru_4O_{12}$(A=Na, Ca, Sr, La, Nd)," *Chem. Phys. Lett.*, **370** [5] 719–24 (2003).

[41]M. H. Whangbo and M. A. Subramanian, "Structural Model of Planar Defects in $CaCu_3Ti_4O_{12}$ Exhibiting a Giant Dielectric Constant," *Chem. Mater.*, **18**, 3257–60 (2006).

[42]L. Wu, Y. Zhu, S. Park, S. Shapiro, G. Shirane, and J. Tafto, "Defect Structure of the High-Dielectric-Constant Perovskite $CaCu_3Ti_4O_{12}$," *Phys. Rev. B*, **71**, 1014118, 8pp (2005).

[43]O. F. Schirmer, "Jahn-Teller Polarons in Oxide Perovskites," *Ferroelectrics*, **303**, 729–33 (2004).

[44]T. T. Fang, L. T. Mei, and H. F. Ho, "Effects of Cu Stoichiometry on the Microstructures, Barrier-Layer Structures, Electrical Conduction, Dielectric Responses, and Stability of $CaCu_3Ti_4O_{12}$," *Acta Mater.*, **54**, 2867–75 (2006).

[45]B. Cheng, Y. H. Lin, H. Yang, J. Lan, C. Nan, X. Xiao, and J. Hey, "High Dielectric Permittivity Behavior in Cu-Doped $CaTiO_3$," *J. Am. Ceram. Soc.*, **92** [11] 2776–9 (2009).

[46]D. Capsoni, M. Binia, V. Massarottia, G. Chiodelli, M. C. Mozzatic, and C. B. Azzonic, "Role of Doping and CuO segregation in Improving the Giant Permittivity of $CaCu_3Ti_4O_{12}$," *J.Solid State Chem.*, **177**, 4494–500 (2004).

[47]F. A. Kröger and H. J. Vink, "Relations Between the Concentrations of Imperfections in Solids," *J. Phys. Chem. Sol.*, **5** [3] 208–23 (1958).

[48]M. L. Moreira, E. C. Paris, G. S. do Nascimento, V. M. Longo, J. R. Sambrano, V. R. Mastelaro, M. I. B. Bernardi, J. Andres, J. A. Varela, and E. Longo, "Structural and Optical Properties of $CaTiO_3$ Perovskite-Based Materials Obtained by Microwave-Assisted Hydrothermal Synthesis: An Experimental and Theoretical Insight," *Acta Mater.*, **57** 5174–85 (2009).

[49]M. A. Gomez, M. A. Griffin, S. Jindal, K. D. Rule, and V. R. Cooper, "The Effect of Octahedral Tilting on Proton Binding Sites and Transition States in Pseudo-Cubic Perovskite Oxides," *J. Chem. Phys.*, **123** [11] 094703, 10pp (2005).

[50]R. V. Vedrinskii, V. L. Kraizman, A. A. Novakovich, P. V. Demekhin, and S. V. Urazhdin, "Pre-Edge Fine Structure of the 3d Atom K X-Ray Absorption Spectra and Quantitative Atomic Structure Determinations for Ferroelectric Perovskite Structure Crystals," *J. Phys. Condens. Matter.*, **10** [42] 9561–80 (1998).

[51]C. Ribeiro, C. Vila, D. B. Stroppa, V. R. Mastelaro, J. Bettini, E. Longo, and E. R. Leite, "Anisotropic Growth of Oxide Nanoparticles: Insights into the Rutile TiO_2 Phase," *J. Phys. Chem.C*, **111** 5871–5 (2007).

[52]V. Krayzman, I. Levin, J. C. Woicik, D. Yoder, and D. A. Fischer, "Effects of Local Atomic Order on the Pre-edge Structure in the TiK X-Ray Absorption Spectra of Perovskite $CaTi_{1-x}Zr_xO_3$," *Phys. Rev. B*, **74** [22] 224104, 7pp (2006).

[53]E. R. Leite, F. M. Pontes, E. C. Paris, C. A. Paskocimas, E. J. H. Lee, E. Longo, P. S. Pizani, J. A. Varela, and V. Mastelaro, "Amorphous Lead Titanate: A New Wide-Band Band Gap Semiconductor with Photoluminescence at Room Temperature," *Adv. Mater. Opt. Electronics*, **10**, 235–40 (2000).

[54]S. de Lazaro, J. Milanez, A. T. de Figueiredo, V. M. Longo, V. R. Mastelaro, F. S. De Vicente, A. C. Hernandes, J. A. Varela, and E. Longo, "Relation Between Photoluminescence Emission and Local Order-Disorder in the $CaTiO_3$ Lattice Modifier," *Appl. Phys. Lett.*, **90**, 111904, 3pp (2007).

[55]J. Milanez, A. T. de Figueiredo, S. de Lazaro, V. M. Longo, R. Erlo, V. R. Mastelaro, R. W. A. Franco, E. Longo, and J. A. Varela, "The Role of Oxygen Vacancy in the Photoluminescence Property at Room Temperature of the $CaTiO_3$," *J. Appl. Phys.*, **106** 043526 (2009).

[56]L. S. Cavalcante, J. C. Sczancoski, J. W. M. Espinosa, J. A. Varela, P. S. Pizani, and E. Longo, "Photoluminescent Behavior of $BaWO_4$ Powders Processed in Microwave-Hydrothermal," *J. Alloy. Compd.*, **474** [1–2] 195–200 (2009).

[57]S. K. Rout, L. S. Cavalcante, J. C. Sczancoski, T. Badapanda, S. Panigrahi, M. S. Li, and E. Longo, "Photoluminescence propertyof ba($Zr_{0.25}Ti_{0.75}$)O_3 Powders Prepared by a Solid State Reaction and Polymeric Precursor Method," *Phys. B*, **404** 3341–7 (2009).

[58]D. L. Wood and J. Tauc, "Weak Absorption Tails in Amorphous Semiconductors," *Phys. Rev. B*, **5** [8] 3144–51 (1972).

[59]S. B. Fagan, A. G. Souza Filho, A. P. Ayala, and J. Mendes Filho, "*Ab Initio* Calculations of $CaCu_3Ti_4O_{12}$ Under High Pressure: Structural and Electronic Properties," *Phys. Rev. B*, **72** 014106, 5pp (2005).

[60]M. Matos and L. Walmsley, "Cation-Oxygen Interaction and Oxygen Stability in $CaCu_3Ti_4O_{12}$ and $CdCu_3Ti_4O_{12}$ Lattices," *J. Phys. Condens. Matter*, **18** [5] 1793–803 (2006).

[61]J. C. Zheng, A. I. Frenkel, L. Wu, J. Hanson, W. Ku, E. S. Bozin, S. J. L. Billinge, and Y. M. Zhu, "Nanoscale Disorder and Local Electronic Properties of CaCu(3)Ti(4)O(12): An Integrated Study of Electron, Neutron, and X-Ray Diffraction, X-Ray Absorption Fine Structure, and First-Principles Calculations," *Phys. Rev. B*, **81** [14] 144203, 19pp (2010).

[62]F. M. Pontes, C. D. Pinheiro, E. Longo, E. R. Leite, S. R. de Lazaro, J. A. Varela, P. S. Pizani, T. M. Boschi, and F. Lanciotti, "The Role of Network Modifiers in the Creation of Photoluminescence in $CaTiO_3$," *Mater. Chem. Phys.*, **78**, 227–33 (2003). □